

Pseudomagnetic fields and ballistic transport in a suspended graphene sheet

M. M. Fogler,¹ F. Guinea,² and M. I. Katsnelson³

¹Department of Physics, University of California San Diego, La Jolla, 9500 Gilman Dr. CA 92093, USA

²Instituto de Ciencia de Materiales de Madrid (CSIC), Sor Juana Inés de la Cruz 3,

Madrid 28049, Spain and Donostia International Physics Center (DIPC),

Paseo Manuel de Lendizabal 4, San Sebastian, E-20018, Spain

³Institute for Molecules and Materials, Radboud University Nijmegen,

Heijendaalseweg 135, 6525 AJ, Nijmegen, The Netherlands

We study a suspended graphene sheet subject to the electric field of a gate underneath. We compute the elastic deformation of the sheet and the corresponding effective gauge field, which modifies the electronic transport. In a clean system the two-terminal conductance of the sample is reduced below the ballistic limit and is almost totally suppressed at low carrier concentrations in samples under tension. Residual disorder restores a small finite conductivity.

Introduction. Graphene layers which are one or a few carbon atoms thick [1, 2] combine novel electronic energy spectrum ("massless Dirac fermions" [3, 4]) and unusual structural and mechanical properties [5, 6, 7, 8, 9] (for a general review, see Refs. 10, 11, 12). Originally, graphene sheets lying on quartz substrate have been prepared and investigated but later it turned out that the freely hanged membranes of macroscopically large sizes can be derived [5]. The electronic transport and mechanical properties of these membranes are being intensively studied [6, 7, 8, 9, 13, 14, 15, 16]. They demonstrate, in particular, a much higher electron mobility, at least, at low temperatures, than graphene sheets on a substrate [13, 14, 16] and extraordinary mechanical stiffness [8], which makes them especially interesting for applications. However, peculiarities of the freely hanged graphene membranes are still poorly understood theoretically.

In this paper we demonstrate that unavoidable deformations of the membranes by an applied electric field can strongly affect their transport properties. The system we consider is sketched in Fig. 1 (a). The calculated deformation h_0 and conductance G are shown in Figs. 2 and 3. The left panel of Fig. 2 shows the maximum deformation as function of carrier density n and slack L in the

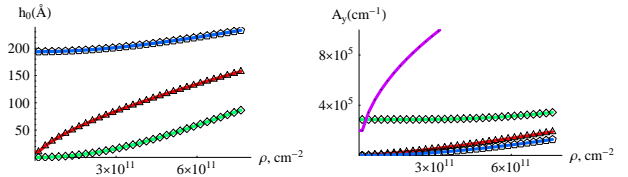


FIG. 2: (Color online) Left: Maximum height, h_0 , for a suspended sheet of length $l = 1 \text{ m}$ as function of carrier density for different slacks: $L = 2 \text{ nm}$; pentagons (blue), $L = 0$, triangles (red), and $L = -2 \text{ nm}$, diamonds (green). Right: Effective gauge field for the same three values of slack. The full magenta curve gives the Fermi wavevector, k_F .

sheet. We define slack as the difference of the equilibrium length of the suspended sheet and the distance between the clamped ends. Negative L implies that the sheet is under tension (see below). The right panel of Fig. 2 gives G as function of carrier density for the same three values of slack. In the presence of a finite deformation parametrized by the maximum vertical displacement h_0 , the conductance is reduced. We found that at not too small carrier concentrations n , function $G(n)$ is given by

$$G \sim \frac{4e^2 W}{h} \frac{k_F}{2} \frac{1}{2} \frac{A_y}{k_F} ; \quad (1)$$

where W is the width of the sample, $k_F = \frac{p}{\hbar}$ is the Fermi wavevector, and A_y of dimension of inverse length is related to the deformation [Eq. (4)]. For graphene initially under tension [9], where h_0 is nearly constant, and low carrier concentrations, we find a nearly complete suppression of transport. The physical mechanism of this phenomenon can be understood as follows. The deformation shifts the Dirac points by the amount A_y [Fig. 1 (b)], which creates a mismatch between the graphene leads and the suspended region. If this shift exceeds the diameter $2k_F$ of the Fermi circle, the electrons are fully reflected.

Recent experiments [16] show a qualitative agreement with our Fig. 3; however, at very low n the conductivity

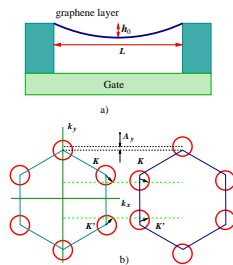


FIG. 1: (Color online). (a) Sketch of the model of a suspended graphene sheet under consideration. (b) Fermi circles positions in the Brillouin zone in the leads (left) and in the suspended region (right).

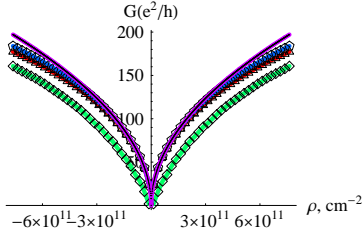


FIG. 3: (Color online) Conductance as function of carrier density. The values of L and the corresponding symbols are the same as in Fig. 2. The full magenta line gives the ballistic conductance in the absence of deformation. The width of the sheet is $W = 1 \text{ nm}$.

saturates at a finite value $\mathcal{E} = h_0$. We attribute this to residual disorder-assisted tunneling processes.

The model. We consider a strip of graphene clamped at two parallel edges $x = \pm L/2$, see Fig. 1. We assume that the width of the strip in the undeformed state is $L + \Delta L$, where ΔL can be of either sign. The strip is suspended above a control gate, whose electric field induces electron concentration n in graphene and exerts on it the pressure $P = (2e^2 n^2)/\epsilon$.

The resultant height profile $h(x)$ of the strip has a well known analytic form [17] under the condition $h_0 \ll L$ where the linear elasticity theory applies. We focus on the case where n is either comparable or much larger than $n_0 = \frac{16\pi}{(16\pi)^2} (\frac{1}{\epsilon}) = (\frac{e^2 L^3}{6 \cdot 10^9 \text{ cm}^2}) = (L/1 \text{ nm})^{3/2}$, where 1.1 eV is the bending rigidity of graphene [18]. In this case the deformation is nearly parabolic:

$$h(x) \approx h_0 + \frac{4x^2}{L^2}; \quad \frac{L}{2} \leq x \leq \frac{L}{2} + \frac{\ln u}{u}; \quad (2)$$

where $u = (n/n_0)(L/h_0)^{1/2} \gg 1$. The maximum deformation h_0 is the positive root of the cubic equation

$$h_0^2 - \frac{3}{16}L - h_0 = \frac{3}{64} \frac{e^2}{E} (nL^2)^2; \quad (3)$$

where $E = 22 \text{ eV}/\text{\AA}^2$ is the Young's modulus of graphene [8]. The values of h_0 for different values of the slack are plotted in Fig. 2.

The deformation of the strip induces perturbations of two types acting on electrons: the scalar potential $V(x)$ and the effective vector potential [19, 20] $A(x)$. We examine these potentials below, starting with $A(x)$.

Vector potential. The aforementioned shift of the Dirac points [Fig. 1(b)] is equivalent to the effect of a constant vector potential $A = (A_x; A_y)$. We use this latter form although in the following as it can be easily generalized to more complex situations. The role of A is the largest when the "zigzag" direction is along the y -axis. Assuming this is

the case, we obtain

$$A_x(x) = 0; \quad A_y(x) = C_1 \frac{t}{aE} = C_1 \frac{PL^2}{a8Eh_0}; \quad (4)$$

where $t = d \log(\epsilon_0) = d \log(a) - 2$ is the dimensionless electron-phonon coupling parameter, $\epsilon_0 = 3 \text{ eV}$ is the nearest neighbor hopping, $a = 1.4 \text{ \AA}$ is the distance between nearest carbon atoms, $s = 1$ is the valley index, $t' = PL^2/(8h_0)$ is the horizontal component of tension per unit length at the edges, and C_1 is a parameter of order unity which depends on the relative displacements within the unit cell, determined by the microscopic force constants [21]. (Note that $u = L/t' = 4$.) The corresponding effective magnetic field $B(x) = \partial A_y$ consists of two narrow spikes at the edges $x = \pm L/2$ [22].

Transport. To compute the two-terminal conductance G through a graphene sheet we assume perfect semi-infinite graphene leads of the same chemical potential at both ends of the strip. Since the perturbations depend only on x , the k_y momentum is conserved. However, the effective magnetic field at the edges shifts the mechanical momentum, $k_y \rightarrow k_y + A_y \text{ sign}(x)$, of electrons that enter the strip. This leads to a nearly complete reflection of electrons at low density where $k_F < A_y = 2$. Similar effect has been previously examined in the context of transmission of Dirac particles through a region of homogeneous magnetic field [23]. However, the present problem has new qualitative features, see below.

For a constant A_y , the transmission coefficient $T(k_y)$ can be computed analytically:

$$T(k_y) = \frac{k(0)^2 k(A_y)^2}{k(0)^2 k(A_y)^2 + k_F^2 A_y^2 \sin^2[k(A_y)L]}; \quad (5)$$

where $k(q) = \frac{P}{k_F^2} (k_y - q)^2$. If $k(A_y)^2 < 0$, then $k(A_y)$ is pure imaginary, so that $\sin^2[k(A_y)L] = 1$.

$\sin^2[k(A_y)L]$. In this case $T(k_y)$ is exponentially small. The plot of $T(k_y)$ is shown in Fig. 4 using the parametrization $k_y = k_F \sin \theta$ for $-\pi/2 < \theta < \pi/2$ and $n = 2 \cdot 10^{11} \text{ cm}^{-2}$. The transmission is indeed almost zero for a range of incident angles. In addition, we see Fabry-Pérot resonances because of the multiple scattering off the two interfaces. (Such resonances are essentially absent if the field is uniform [23].)

Neglecting the contribution of edge channels, which is permissible when the number of bulk channels $k_F W = 1$ is large, the conductance can be computed from

$$G = \frac{4e^2}{h} W \int_{k_F}^{2k_F} \frac{dk_y}{2} T(k_y); \quad (6)$$

This integral can be done analytically in the limit $k_F \gg A_y$ and $L k_F \gg 1$, see Eq. 1. Using Eqs. (3)-(6), we also computed $G(n)$ numerically for three L shown in Fig. 3. For $L = 0$, where the tension and therefore

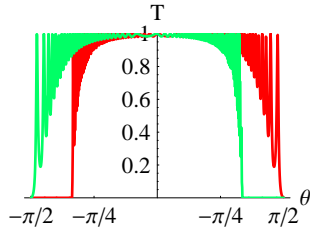


FIG. 4: (Color online). Angular dependence of the transmission for $h_0 = 20$ nm, no slack, and $L = 1$ μ m. The carrier density is $n = 2 \times 10^{11}$ cm $^{-2}$. The two curves correspond to the two inequivalent Dirac points.

β_A rapidly increase with n (Fig. 1), the deviations from the ballistic formula occur at large n . In contrast, for $L = 2$ nm, where the tension is approximately constant, the largest effect of the gauge field is felt at low concentrations, leading to a nearly complete vanishing of G at $|\beta_A| < 2 \times 10^{10}$ cm $^{-2}$.

Disorder effects. Any realistic system contains disorder. When weak, it does not change qualitatively the above results for $G(n)$ at high carrier concentration $|\beta_A| \gg \beta_y$. In the opposite limit, when G is strongly suppressed, the effect of disorder is important because it relaxes the constraint of momentum conservation, compensating for the momentum shift due to the gauge field at the interfaces $x = \pm L/2$.

Consider the experimentally relevant case [16] where the elastic mean-free path l is comparable to the system size L . Then, at $l \approx G = (4e^2/h) k_F W$ we have a regime where the disorder is weak enough that its effect on the average conductance is still negligible yet it is strong enough to fully mix the transverse modes in the suspended region. In this case the conductance is limited by the two interfaces, which act as classical resistors in series [24], $G = G_i = 2$. Let us compute the conductance of a single interface G_i with and without including the effect of disorder.

If disorder near the interface is neglected, G_i is given by the expression similar to Eq. (6) where $T(k_y)$ is now the transmission coefficient through a single interface: $T(k_y) = [k(0)k(A)] / [(k(0) + k(A))^2 + A_y^2]$. This formula holds if k_y -mode is propagating, $k(0) = k(A) = 0$. Otherwise, it is evanescent and $T(k_y) = 0$. Each evanescent mode decays exponentially either to the left or to the right of $x = 0$ interface, depending on which of $k(0)$ and $k(A)$ is nonzero. At $k_F < \beta_A/2$ all modes at the Fermi energy are evanescent. Therefore, if the disorder is neglected, G_i vanishes.

Let us now include disorder-induced mixing among the evanescent and propagating modes, which gives a correction $\delta T(k_y)$ to each $T(k_y)$. To the lowest order in the concentration n_s of scatterers, this correction can be

written as

$$T(k_y) = \frac{A_y}{2} \int_{-k_F}^{k_F} dk_y^0 \int dx n_s T(k_y; k_y^0; x); \quad (7)$$

where $T(k_y; k_y^0; x)$ is the off-diagonal transmission coefficient due to a single scatterer at position $r = (x; y)$. Function $T(k_y)$ has the dimension of length, similar to the transport cross-section $\sigma_s = l/(n_s l)$. On physical grounds, we expect $T(k_y; k_y^0; x) \propto (k_y - k_y^0) \exp(-2\beta_A |x|)$. Here the exponential represents the probability of the evanescent wave to reach the scatterer and the prefactor provides the correct units and scaling with disorder strength. The dominant contribution to $T(k_y)$ comes from the scatterers located in the strip $|\beta_A| \approx |\beta_A|$. Integrating over x , k_y , and k_y^0 , we finally get

$$G = \frac{G_i}{2} = \frac{4e^2}{h} \frac{k_F W}{2\beta_A l} = \frac{e^2}{h} \frac{4C_2 W n}{\beta_A l(n)}; \quad (8)$$

where C_2 is a numerical coefficient and $l(n)$ is the conductivity of a sample with size $L \approx 1$. A formal derivation based on the Green's function formalism yields $C_2 = 4$. For estimate, we can take $n = 10^9$ cm $^{-2}$, $4e^2/h$, $W = 1$ μ m, and $\beta_A = 2 \times 10^5$ cm $^{-1}$. We then find $G \approx 2e^2/h$, i.e., an appreciably large value.

Scalar potential. The deformation of the graphene strip also creates a scalar potential $V(x)$ in the system. Our estimates below indicate that it is relatively small, so that its presence is not expected to change the results shown in Figs. 3 and 4 in a major way. We will discuss it briefly, for completeness.

The bare potential induced by the deformation is:

$$V_{\text{ext}}(x) = \frac{Ph(x)}{en} + V_0(u_{xx} + u_{yy}) \\ = \frac{Ph(x)}{en} + \frac{L}{2} |\beta_A| \frac{tV_0}{E}; \quad (9)$$

where the first term is the change in electrostatic potential due to the change in distance to the gate, the second term gives the deformation potential induced by a local compression [21, 25] $u_{xx} + u_{yy}$, and $V_0 \approx 10$ eV.

Within the linear screening theory, the Fourier transform \tilde{V} of V is given by $\tilde{V}(q) = \tilde{V}_{\text{ext}}(q) = \tilde{V}(q)$, where $\tilde{V}(q)$ is the dielectric function. For reasonable carrier concentrations, the potential in Eq. (9) is smooth over distances $k_F^{-1} \ll L$. We can use the Thomas-Fermi (TF) approximation, $\tilde{V}(q) = 1/k_s + \tilde{V}$, where $k_s = 4k_F$ is the inverse TF screening length and $\tilde{V} = e^2/\epsilon$ is the dimensionless strength of the Coulomb interaction. The screened potential can be computed analytically in terms of special functions. In the limit $k_s L \gg 1$ and at dis-

tances greater than k_s^{-1} from the boundaries it reads:

$$eV(x) = \frac{1}{2} \frac{PV_0}{Eh_0k_s} \frac{L^3}{L^2 - 4x^2} - \frac{8Ph_0}{nk_sL} \left[1 + \frac{x}{L} \ln \frac{L}{L+2x} \right] \quad (10)$$

The potential at the edge is given by

$$eV\left(\frac{L}{2}\right) = \frac{PV_0L^2}{16Eh_0} + \frac{4Ph_0}{nk_sL} [C_3 - \ln(k_sL)]; \quad (11)$$

where $C_3 = 1$. Thus, the divergences in Eq. (10) are cut off at the distance of the order of the screening length $l=k_s^{-1}$ from the edge, as expected.

For $n = 3 \cdot 10^{11} \text{ cm}^{-2}$, the deformation and the electrostatic potentials at the edges are comparable in magnitude and together amount to about 10% of the Fermi energy. Although this is not a negligible amount, it is still numerically small, so that the linear-response screening approach is justified.

Experimental implications and future directions. In this paper we focused on a simplest geometry of a suspended graphene strip (Fig. 1) for which the calculation of the transport properties can be done semi-analytically. We have found that reasonable values of the tension, $L=L_0 \pm 0.2\%$ in a suspended graphene strip can lead to the almost total reflection for a significant range of incoming momenta, which causes a downward shift of the two-terminal conductance compared to the ballistic limit, Eq. (1). Residual disorder can partially compensate for this shift, which may be the case in current experiments [13, 14, 16]. Note however, that our theory cannot be directly compared with experiments, as the sample geometry and therefore the configuration of the gauge field can be more complicated than what we have assumed here.

There are a number of possible directions for future study. One interesting problem is how the deformation would affect the quantum Hall effect (QHE) in the suspended graphene. Below we offer a preliminary discussion of this question.

For the model considered, the effects of the deformation are restricted to the $x = \pm L/2$ interfaces. The Landau levels near such lines will be modified (except for the $N = 0$ one, which is topologically protected [26, 27]). Quasiclassically, the reflection at the interfaces creates skipping orbits, which propagate parallel to the y -axis but in opposite directions on the two sides of each interface. This could lead to backscattering of the edge currents and modification of the QHE. The effect is the strongest when $k_F \approx \beta_y j$. For low-lying Landau levels, where $k_F \approx l = \frac{1}{k_s}$, an estimate of the external magnetic field B below which the QHE is affected can be derived from the condition $l_B(B) \approx \beta_y j$. For $L = 2 \text{ nm}$, and $A_y = 2 \cdot 10^{10} \text{ cm}^{-1}$, it yields $B \approx 0.7 \text{ T}$.

In a more realistic geometry, a small fictitious magnetic field will also exist inside the suspended region. Its magnitude is of the order of 0.05 T for the same L and L . Landau levels mixing in the bulk occurs when the external field is comparable or smaller than this value.

This work was supported by MEC (Spain) through grant FIS2005-05478-C02-01 and CONSOLIDER CSD2007-00010, the Comunidad de Madrid, through CITECNOM IK, CM2006-S-0505-ESP-0337, the EU Contract 12881 (NEST), the Stichting voor Fundamenteel Onderzoek der Materie (FOM) (the Netherlands), and by the US NSF under grant DMR-0706654. We appreciate helpful conversations with M. A. H. Vozmediano.

-
- [1] K. S. Novoselov et al., *Science* 306, 666 (2004).
 - [2] K. S. Novoselov et al., *Proc. Natl. Acad. Sci. U.S.A.* 102, 10451 (2005).
 - [3] K. S. Novoselov et al., *Nature* 438, 197 (2005).
 - [4] Y. Zhang, Y.-W. Tan, H. L. Stormer, and P. Kim, *Nature* 438, 201 (2005).
 - [5] J. C. Meyer et al., *Nature* 446, 60 (2007).
 - [6] J. S. Bunch et al., *Science* 315, 5811 (2007).
 - [7] D. Garcia-Sanchez et al., *Nano Lett.* 8, 1399 (2008).
 - [8] T. J. Booth et al., *Nano Lett.* (2008), DOI: 10.1021/nl801412y.
 - [9] J. S. Bunch et al. (2008), arXiv:0805.3309.
 - [10] A. K. Geim and K. S. Novoselov, *Nature Materials* 6, 183 (2007).
 - [11] M. I. Katsnelson and K. S. Novoselov, *Sol. St. Commun.* 143, 3 (2007).
 - [12] A. H. Castro Neto, F. Guinea, N. M. R. Peres, K. S. Novoselov, and A. K. Geim (2008), *Rev. Mod. Phys.*, in press, arXiv:0709.1163.
 - [13] K. I. Bolotin et al., *Sol. St. Commun.* 156 (2008).
 - [14] X. Du, I. Skachko, A. Barker, and E. Y. Andrei (2008), arXiv:0802.2933.
 - [15] G. Li, A. Luican, and E. Y. Andrei (2008), arXiv:0803.4016.
 - [16] K. I. Bolotin et al. (2008), arXiv:0805.1830.
 - [17] S. P. Timoshenko and S. Woinowsky-Krieger, *Theory of Plates and Shells* (McGraw-Hill, New York, 1959).
 - [18] A. Fasolino, J. H. Los, and M. I. Katsnelson, *Nature Materials* 6, 858 (2007).
 - [19] S. V. Morozov et al., *Phys. Rev. Lett.* 97, 016801 (2006).
 - [20] J. L. Mañes, *Phys. Rev. B* 76, 045430 (2007).
 - [21] H. Suzuura and T. Ando, *Phys. Rev. B* 65, 235412 (2002).
 - [22] The total stress tensor includes contributions from the in-plane and out-of-plane displacements, and it is constant within the deformed region, see F. Guinea, B. Horovitz and P. Le Doussal, *Phys. Rev. B* 77, 205421 (2008).
 - [23] A. D. Martino, L. Dell'Anna, and R. Egger, *Phys. Rev. Lett.* 98, 066802 (2007).
 - [24] C. W. J. Beenakker, *Rev. Mod. Phys.* 3, 731 (1997).
 - [25] S. Ono and K. Sugihara, *J. Phys. Soc. Jap.* 21, 861 (1966).
 - [26] A. J. M. Giesbers et al., *Phys. Rev. Lett.* 99, 206803

(2007).

[27] F. Guinea, M. I. Katsnelson, and M. A. H. Vozmediano,

Phys. Rev. B 77, 075422 (2008).